Available online at www.sciencedirect.com

ScienceDirect

Geochimica et Cosmochimica Acta 276 (2020) 258–273

Geochimica et Cosmochimica Acta

www.elsevier.com/locate/gca

Oxygen and clumped isotope fractionation during the formation of Mg calcite via an amorphous precursor

Martin Dietzel [a,*], Bettina Purgstaller [a], Tobias Kluge [c,e], Albrecht Leis [b], Vasileios Mavromatis [a,d]

[a] Graz University of Technology, Institute of Applied Geosciences, Rechbauerstrasse 12, 8010, Graz, Austria
[b] JR-AquaConSol GmbH, Steyrergasse 21, 8010, Graz, Austria
[c] Institute of Environmental Physics, Heidelberg University, Im Neuenheimer Feld 229, 69120 Heidelberg, Germany
[d] Géosciences Environnement Toulouse (GET), CNRS, UMR 5563, Observatoire Midi-Pyrénées, 14 Av. E. Belin, 31400 Toulouse, France
[e] Institute of Applied Geosciences, Karlsruhe Institute of Technology, Adenauerring 20 b, 76131 Karlsruhe, Germany

Received 8 November 2019; accepted in revised form 25 February 2020; available online 4 March 2020

Abstract

The oxygen and clumped isotope signatures of Mg calcites are routinely used as environmental proxies in a broad range of surroundings, where Mg calcite forms either by classical nucleation or via an amorphous calcium magnesium carbonate (ACMC) precursor. Although the (trans)formation of ACMC to Mg calcite has been identified for an increasing number of settings, the behavior of both isotope proxies throughout this stage is still unexplored. In the present study ACMC (trans)-formation experiments were carried out at constant pH (8.30 ± 0.03) and temperature (25.00 ± 0.03 °C) to yield high Mg calcite (up to 20 mol% Mg). The experimental data indicate that the oxygen isotope values of the amorphous and/or crystalline precipitate ($\delta^{18}O_{prec}$, analyzed as Mg calcite) are affected by the (trans)formation pathway, whereas clumped isotopes ($\Delta_{47prec} = \Delta_{47Mg\text{-}calcite}$) are not. The oxygen isotope evolution of the solid phase can be explained by the instantaneous trapping of the isotopic composition of the aqueous (bi)carbonate complexes. This entrapment results in remarkably high $10^3\ln(\alpha_{prec\text{-}H2O})$ values of ~33‰ at the initial ACMC formation stage. During the ACMC transformation process the oxygen isotope equilibrium is approached rapidly between Mg calcite and water ($\Delta^{18}O_{Mg\ calcite\text{-}water} = 30.3 \pm 0.4$‰) and no isotopic memory of the initial to the final Mg calcite at the end of the experiment occurs. The implications for oxygen and clumped isotope signatures of Mg calcite formed via ACMC are discussed in the aspects of various scenarios of (trans)formation conditions and their use as environmental proxies.

Keywords: Oxygen isotope fractionation; Clumped isotopes; Amorphous calcium magnesium carbonate; Mg calcite; Transformation

1. INTRODUCTION

Oxygen- and clumped- isotope signatures of carbonate minerals are used as environmental proxies in a broad range of tasks comprising ancient ocean composition, paleoclimate reconstruction, origin of life- and dolostone, carbonate diagenesis, speleothem formation, hydrothermal carbonate deposits, technical settings, geochemical forensics etc. (e.g. Dietzel et al., 1992; Kosednar et al., 2008; Hoefs, 2015 and references therein; Defliese et al., 2016; Dietzel et al., 2016; Falk et al, 2016; Spooner et al., 2016; Fohlmeister et al., 2018; Kluge et al., 2018; Boch et al., 2019). To date oxygen isotope fractionation between calcite and water and clumped isotopes of calcite were studied via direct precipitation from an aqueous solution. In the past two decades, however, an alternative pathway of calcite formation has been shown to occur. During this mode of

* Corresponding author.
E-mail address: martin.dietzel@tugraz.at (M. Dietzel).

https://doi.org/10.1016/j.gca.2020.02.032
0016-7037/

precipitation a metastable amorphous calcium carbonate (ACC) precursor forms initially and subsequently transforms to a crystalline $CaCO_3$ phase. The presence of ACC precursors has been shown to occur in many environmental settings, e.g. calcifying organisms, speleothems and also in man-made settings like carbonate binder formation (e.g. Demény et al., 2016; Konrad et al., 2016; Ševčík et al., 2016; Carino et al., 2017; Jacob et al., 2017; Mass et al., 2017; Jin et al., 2018). In most natural settings, ACC precursors are formed in the presence of Mg ions – the most common and important cation substituting Ca in the calcite structure – resulting in a more general precursor phase: amorphous calcium magnesium carbonate (ACMC; Albéric et al., 2018; Purgstaller et al., 2019).

The presence of an ACMC precursor has been shown to exert significant controls on the mineralogy and the chemical/isotopic composition of the forming crystalline carbonate (e.g. Konrad et al., 2018). For example the presence of an ACMC precursor allows the incorporation of elevated amounts of Mg in the calcite crystal structure. Indeed, high Mg calcite ($MgCO_3 > 4$ mol%) is rather unlikely to form via classic overgrowth techniques (Mavromatis et al., 2013; Goetschl et al., 2019). In contrast, recent studies focused on the precipitation of ACMC have shown that its transformation results in high Mg calcites with up to 20 mol% $MgCO_3$ at 25 °C (Loste et al., 2003; Purgstaller et al., 2016) and proto-dolomite at >40 °C (Schmidt et al., 2005; Rodriguez-Blanco et al., 2015). In addition to the mineralogy and chemical composition, the presence of an ACMC precursor during the formation of Mg-bearing calcite has been shown to affect its isotopic composition. Indeed, in the earlier study by Mavromatis et al. (2017a), high Mg-calcites formed via an amorphous precursor achieve near equilibrium values with respect to Mg isotopes, almost immediately after the transformation of the ACMC precursor to the crystalline phase. This contrasts earlier studies, where Mg-calcite precipitated on seed material, and mineral growth kinetics control the isotopic composition of the forming solid (Mavromatis et al., 2013; 2017b).

Although the presence of an amorphous precursor is considered to play a role in the formation of Mg calcite in many natural surroundings, the oxygen and clumped isotope fractionation between amorphous (ACMC), crystalline precipitate (Mg calcite) and water is still not experimentally evaluated. The present study explores the oxygen and clumped isotope fractionation behavior between precipitate and solution during the formation of ACMC and its transformation to Mg calcite at well-defined physicochemical conditions ($pH = 8.30 \pm 0.03$; $T = 25.00 \pm 0.03$ °C). In the approach used herein, the evolution of both isotope signatures is investigated as a function of precipitation/transformation time. The obtained results evaluate the potential effects of an amorphous precursor pathway on the oxygen isotope and clumped signatures of the final Mg calcite and how these isotope proxies might be used to estimate (trans)formation temperatures or trace Mg calcite formation mechanisms and pathways.

2. THEORETICAL CONSIDERATIONS

The application of traditional oxygen isotopes is based on the temperature dependence of the oxygen isotope fractionation between a carbonate mineral, like calcite, and the precipitating solution according to the overall exchange reaction

$$1/3\ CaC^{18}O_3 + H_2{}^{16}O = 1/3\ CaC^{16}O_3 + H_2{}^{18}O \quad (1)$$

(e.g. Urey, 1947; McCrea, 1950; O'Neil et al., 1969; Kim and O'Neil, 1997). Thus, the oxygen isotopic composition of carbonate minerals is routinely used as (paleo)temperature proxy assuming that the oxygen isotopic composition of the carbonate precipitating solution is known or can be reasonable estimated in marine or terrestrial environments (e.g. for calcite: Epstein et al., 1953; Hendy, 1971; Veizer et al., 1999; Adkins et al., 2003; Hoefs, 2015 and references therein). In contrast clumped isotope signatures are based on the multiply-substituted isotopologues in carbonates according to the equation

$$Ca^{12}C^{18}O^{16}O_2 + Ca^{13}C^{16}O_3 = Ca^{13}C^{18}O^{16}O_2 + Ca^{12}C^{16}O_3 \quad (2)$$

(e.g. for calcite; Eiler, 2007; Schauble et al., 2006) forming temperature-dependent stochastic abundances of the ^{13}C–^{18}O bonds. This approach provides a temperature proxy, which is independent of the isotopic composition of the precipitating solution and widely used for calibration studies and re-constructing of environmental surroundings of carbonate mineral formation (e.g. Ghosh et al, 2006; Kluge et al., 2015; Kluge et al., 2018; Kele et al., 2015; Defliese et al., 2016; Piasecki et al., 2019; Guo et al., 2019). For the application of both these approaches isotopic equilibrium in respect to the isotopic distribution between the precipitate, here Mg calcite, and the aqueous species has to be reached, which is particularly challenging at ambient and low temperatures (e.g. Dietzel et al., 2009; Burgener et al., 2018; Daëron et al., 2019).

The oxygen isotope fractionation coefficient between a carbonate mineral – shown here for calcite as the solid phase – and water is given by the expression

$$\alpha_{calcite-water} = \frac{{}^{18}R_{calcite}}{{}^{18}R_{water}} = \frac{n_{calcite}({}^{18}O)/n_{calcite}({}^{16}O)}{n_{water}({}^{18}O)/n_{water}({}^{16}O)} = \frac{\delta\ {}^{18}O_{calcite} + 1000}{\delta\ {}^{18}O_{water} + 1000} \quad (3)$$

and is accordingly defined by the n moles of ^{18}O and ^{16}O of the solid carbonate (calcite) divided by the n moles of ^{18}O and ^{16}O of the precipitating water (H_2O; see Eq. (1)). An isotope fractionation coefficient, $\alpha_{calcite\text{-}water}$, that is closest to isotope equilibrium conditions was estimated using speleothem calcite grown at very low precipitation rates ($\alpha_{calcite\text{-}water} = 1.0302$; $10^3\ln(\alpha_{calcite\text{-}water} = 29.8‰$ at 25 °C; see data given by Coplen (2007) and Daëron et al. (2019). Kinetically driven oxygen isotope fractionation effects can be related to non-isotopically equilibrated dissolved inorganic carbonate (DIC) species and/or high precipitation rates (e.g. Dietzel et al., 2009; Geisler et al., 2012; Tripati et al., 2015; Watkins and Hunts, 2015). Both effects are

known to result in lower apparent $\alpha_{calcite\text{-}water}$ values compared to equilibrium conditions. In brief, these kinetic effects are reflecting isotopic disequilibrium conditions between the aqueous DIC species and/or during the uptake of the aqueous carbonate at the growing calcite surface (e.g. Dietzel et al., 2009; Watkins et al., 2013; Tripati et al., 2015).

The clumped isotope signatures are based on the distribution of the rare multiply-substituted isotopologues in the carbonate ion (e.g. Gosh et al., 2006; Eiler, 2007). This stable isotope thermometer is referred to a homogeneous isotope exchange and the measurement of the less abundant ^{13}C and ^{18}O isotopes bonded together in a carbonate molecule ($^{13}C^{18}O^{16}O_2^{2-}$ see Eq. (2)). The clumped isotopic composition of calcite is expressed as:

$$\Delta_{47} = \left[\frac{^{47}R}{2\ ^{13}R \cdot\ ^{18}R + 2\ ^{17}R \cdot\ ^{18}R +\ ^{13}R \cdot (\ ^{17}R)^2} - \frac{^{46}R}{2\ ^{18}R + 2\ ^{13}R \cdot\ ^{17}R + (\ ^{17}R)^2} - \frac{^{45}R}{^{13}R + 2\ ^{17}R} + 1 \right] \quad (4)$$

and it is based on the deviation of the measured ^{13}C–^{18}O abundance from stochastic distribution at very high temperature (e.g., Kluge et al., 2015). The $\Delta_{47calcite}$ value is calculated from the ratios $^{i}R = {}^{i}R_{calcite}$ of masses i = 13, 18, 45, etc.. At 25 °C $\Delta_{47calcite}$ values at near isotope equilibrium conditions are documented from laboratory calibrations and natural deposits: e.g. $\Delta_{47calcite} = 0.702$; 0.700; 0.695, 0.660 from Zaarur et al. (2013), Kele et al. (2015), Kluge et al. (2015), Daëron et al. (2019), respectively. The latter value is measured in speleothem calcite formed at very slow precipitation rates, thus most likely approaching isotopic equilibrium. Deviation of $\Delta_{47calcite}$ values for precipitated calcite from isotope equilibrium is mostly referred to non-equilibrated DIC, likely caused by CO_2 hydration/hydroxylation effects in particular at alkaline pH (e.g. Hill et al., 2014; Tang et al., 2014; Tripati et al., 2015; Watkins and Hunts, 2015; Sade and Halevy, 2017; Bajnai et al., 2018; Guo, 2019).

3. METHODOLOGY

3.1. Experimental setup

The experimental setup used for the precipitation and transformation of amorphous calcium magnesium carbonate is described in detail in Purgstaller et al. (2016). Briefly, 50 ml of a 1 M $NaHCO_3$ solution were placed in a stirred 150 ml borosilicate glass reactor, where within 25 min 50 ml of a 0.6 M (Ca,Mg)Cl_2 solution was titrated at a rate of 2 ml min^{-1} at 25.00 ± 0.03 °C (Fig. 1A). The Mg/Ca ratio used in the 0.6 M (Ca,Mg)Cl_2 solution was 1:5 for experiment #MgCa5 and 1:4 for experiment #MgCa4. The pH of the reactive solution was kept constant at pH 8.3 ± 0.1 by automatic titration of a 1 M NaOH solution. After 60 min the suspension was transferred into a 150 mL air-tight glass bottle and which was placed in a shaker at 25 ± 1 °C. As a function of reaction time samples of the suspensions were collected. Subsequently precipitates and solutions were separated by membrane filtration (0.2 µm) for chemical and isotopic analyses. Ultrapure water (Millipore Integral 3: 18.2 MΩcm^{-1}) and analytical grade chemicals were used for solution preparation. The temporal evolution of carbonate precipitates was monitored by *in situ* Raman spectroscopy as well as by continuous sampling and analysis of precipitates and reactive solutions.

3.2. Analytics

3.2.1. Solids and liquids

The mineralogy of the precipitates was monitored *in situ* by Raman Spectroscopy using a RAMAN RXN2^{TM} analyzer from Kaiser Optical Systems (MR Probe head; 785 nm laser beam) at a time-resolution of 35 s. Additionally X-Ray diffraction (XRD; PANanalytical X´Pert Pro diffractometer using Co-Kα) and attenuated total reflection – infrared spectroscopy (ATR-FTIR; Perkin Elmer Spektrum 100) of sampled solids through each run was carried out. The Mg bearing $CaCO_3$ precipitates were characterized for their Mg contents expressed as mol% $MgCO_3$ = $(Mg^{2+})/(Ca^{2+} + Mg^{2+}) \cdot 100$ as calcium and magnesium are the only divalent cations present. The mol % $MgCO_3$ of the precipitates at a given reaction time was calculated according to mass balance considerations based on the evolution of the experimental solution chemical composition, XRD pattern shift (in the case of Mg-calcite), and acid digestions of precipitates. All calculations yield the same value within analytical uncertainty, but due to their lowest uncertainty (±1 mol % $MgCO_3$) acid digestions are used in the present study.

Aqueous cation concentrations were measured using ion chromatography (Dionex IC S 3000) with an analytical precision of ±3 %. The total alkalinity of the solutions was determined by titration using a 0.02 M HCl solution with an analytical precision of ±2 %. The aqueous speciation of the reactive solutions, ion activities and saturation degrees were calculated using the PHREEQC computer code (Parkhurst and Appelo, 1999) with its minteq.v4 database. The ion activity product for $Ca_{1-x}Mg_xCO_3$ ($IAP = (a_{Ca^{2+}})^{1-x}\left(a_{Mg^{2+}}\right)^{x}\left(a_{CO_3^{2-}},\right)$, such as Mg-calcite and ACMC, was calculated from ion activities in the solutions (a_i) and the mole fraction of $MgCO_3$ in the precipitate (x) (see Purgstaller et al., 2016).

3.2.2. Isotopes

The stable oxygen isotope ratios of calcite samples were measured with a Thermo Fisher Scientific (Bremen, Germany) Gas Bench II carbonate preparation device con-

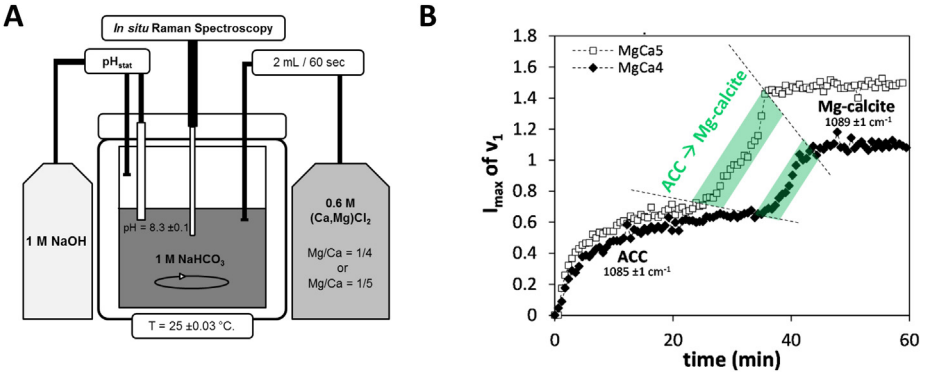

Fig. 1. A: Experimental setup used for the precipitation of calcium magnesium carbonate during the experimental runs #MgCa4 and #MgCa5 at a molar Mg/Ca ratio of 1/4 and 1/5, respectively (adapted from Purgstaller et al., 2016). B: Evolution of the maximum intensity (I_{max}) of the υ_1 vibration band of solid CO_3^{2-} from FTIR spectra as a function of experimental time up to one hour, where individual wave numbers at I_{max} are given. At a reaction time of 25 min mixing of the two stock solution ends. The green shaded areas indicate the transformation period of amorphous calcium magnesium carbonate (ACMC) to Mg calcite (~20% and 16% Mg calcite for the final product at a reaction time of 60 days, respectively) by a rapid increase of I_{max} (see Purgstaller et al., 2016). (For interpretation of the references to colour in this figure legend, the reader is referred to the web version of this article.)

nected to a Finnigan DELTA^{plus} XP isotope ratio mass spectrometer (Révész and Landwehr, 2002; Spötl and Vennemann, 2003). Sample vessels were cleaned with diluted phosphoric acid, then rinsed three times with deionized water (18.2 MΩ·cm^{-1}, ELGA PURELAB Maxima) and dried overnight at 70 °C. Prior to analyses phosphoric acid was injected into the individual sample vials. Each sample was analyzed twice. The dried samples and international reference materials (NBS_19 and NBS_18) were simultaneously measured. The oxygen isotopic composition is reported in the delta notation as the per mil (‰) deviation relative to the Vienna Pee Dee belemnite standard (VPDB) according to the equation

$$\delta\ ^{18}O_{prec} = \frac{^{18}O/^{16}O_{sample} - ^{18}O/^{16}O_{standard}}{^{18}O/^{16}O_{standard}} \times 1000 \qquad (5)$$

The overall precision (2σ) for the measurements of $\delta^{18}O_{prec}$ is ±0.08‰. The oxygen isotopic composition of the sampled experimental solutions in respect to H_2O was analyzed with a Finnigan DELTA^{plus} mass spectrometer using the classic CO_2-H_2O equilibrium method (Horita et al., 1989). The $\delta^{18}O_{water}$ values (±0.05‰) are given relative to Vienna Standard Mean Ocean Water (VSMOW). It has to be noted that the initial experimental $NaHCO_3$ solution is set to isotope equilibrium between H_2O and DIC species with respect to oxygen isotopes by preparing a day before using it for the experiments, as at ambient temperature and pH 8.3 about 10 hours are required to reach isotope equilibrium (e.g. Usdowski et al., 1991; Zeebe and Wolf-Gladow, 2005; Weise and Kluge, 2019). The oxygen isotope fractionation coefficient between precipitated calcite and water defined in equation (3) yield apparent $10^3 ln\alpha_{prec\text{-}water}$ values ($\approx \Delta^{18}O_{prec\text{-}water} = \delta^{18}O_{prec} - \delta^{18}O_{water}$). The latter values are based on isotopic values relative to VSMOW, where the conversion of $\delta^{18}O$ values from VPDB to VSMOW standard is given by $\delta^{18}O$ (VSMOW) = 1.03091 $\delta^{18}O$(VPDB) + 30.91 (e.g. Hoefs, 2015).

For clumped isotope measurements subsamples of the carbonate precipitates were reacted with 105% phosphoric acid in stirred glass vessels at 90 °C for 10 min and the released CO_2 was collected in a nitrogen-cooled glass trap (Kluge et al., 2015). After separation and purification the CO_2 was transferred either to a Finnigan MAT 253 stable isotope ratio mass spectrometer (Thermo Fisher Scientific) at Imperial College, London or a Finnigan MAT 253 Plus (Thermo Fisher Scientific) at Heidelberg University for carbonate clumped isotope analysis. A measurement consisted of eight acquisitions with 10 cycles per acquisition. The clumped isotopic composition is based on the deviation of the measured ^{13}C–^{18}O abundance from stochastic distribution at very high temperature and is given as Δ_{47} value according to equation (4) including gas and carbonate standards as reference and the ^{17}O correction of Daëron et al. (2016). Accordingly, Δ_{47} values are calculated from the measured ratios ($R = R_{calcite}$) of masses 45, 46 and 47 to mass 44 and by calculating ^{13}R ($^{13}C/^{12}C$) and ^{18}R ($^{18}O/^{16}O$) from ^{45}R and ^{46}R assuming random distribution, whereas ^{17}R is calculated from ^{18}R assuming a mass-dependent relationship between ^{18}O and ^{17}O.

All precipitates were dried at 25 °C before $\delta^{18}O$ and Δ_{47} analyses took place to remove water and provide Mg calcite for isotope analyses (verified by XRD pattern), although the precipitate may originally contain ACMC. The latter step was required to get a well-defined material (in this case calcite), where the acid fractionation factor for CO_2 release by adding phosphoric acid is known for re-calculation of isotope values and potential artifacts caused by oxygen isotope exchange of H_2O (included in ACMC) during acidification and CO_2 production can be ruled out. To test whether or not this preparation has an effect on the measured isotope data, selected aliquots of the precipitates from a separately conducted experiment #CaMg4* at a reaction time of 5 min and 24 h, respectively, were kept at 25 and 50 °C for drying (see Table 1). The experiment conditions

Table 1
Experimental data for the precipitation of calcium magnesium carbonate for experimental runs #MgCa4 and #MgCa5 at a molar Mg/Ca ratio of 1/4 and 1/5, respectively, at T = 25 ± 0.1 °C and pH = 8.2 ± 0.1 and at individual run times (see details in Purgstaller et al., 2016). $MgCO_3$ (=Mg/(Ca + Mg) * 100 of the precipitate) denote the Mg content of the ACMC and Mg calcite in % at a reaction time of up to 25 min and 129600 min (90 days), respectively, where the analysed material consists of Mg calcite as a transformation product throughout drying in all runs at 25 °C and for (50) at 50 °C. $\delta^{18}O_{prec}$ and $\delta^{18}O_{water}$: Oxygen isotope composition of precipitate and water. $\alpha_{prec\text{-}H2O}$: Apparent oxygen isotope fractionation between the precipitate and water. $\delta^{18}O_{CO2}$, $\delta^{18}O_{HCO3\text{-}}$, and $\delta^{18}O_{CO32\text{-}}$ values are referred to the oxygen isotope composition of DIC species calculated using measured $\delta^{18}O_{H2O}$ values and isotope equilibrium fractionation factors at equilibrium from literature at 25 °C given in Tab.2. The oxygen isotope composition of the total DIC is obtained by the calculated molar fractions (x) of the dissolved DIC species (from PHREEQC modelling) and their individual oxygen isotopic composition ($\delta^{18}O_{DIC} = x_{CO2}\ \delta^{18}O_{CO2} + x_{HCO3\text{-}}\ \delta^{18}O_{HCO3\text{-}} + x_{CO32\text{-}}\ \delta^{18}O_{CO32\text{-}}$). Δ_{47} denotes the analysed clumped isotope composition of the precipitate and n the number of separate analyses. *separate analogous experiment.

	Time	$MgCO_3$	$\delta^{18}O_{prec}$	$\delta^{18}O_{prec}$	$\delta^{18}O_{water}$	$10^3\ln(\alpha_{prec\text{-}water})$	$\delta^{18}O_{CO2}$	$\delta^{18}O_{HCO3\text{-}}$	$\delta^{18}O_{CO32\text{-}}$	$\delta^{18}O_{DIC}$	$10^3\ln(\alpha_{DIC\text{-}water})$	xCO_2	$xHCO_3^-$	xCO_3^{2-}	Δ_{47}		n
	Min	%	‰ (VPDB)	‰ (VSMOW)	‰ (VSMOW)	(‰)	‰ (VSMOW)	‰ (VSMOW)	‰ (VSMOW)	‰ (VSMOW)	(‰)				‰		
CaMg4	5	4.6	−8.87	21.77	−9.59	31.17	31.31	21.62	14.66	21.50	30.91	0.001	0.980	0.019	0.689	±0.02	1
CaMg4	13	6.8	−7.36	23.32	−9.38	32.48	31.53	21.84	14.88	21.70	30.89	0.001	0.977	0.022	0.710	±0.017	5
CaMg4	25	9.9	−8.56	22.09	−9.21	31.10	31.71	22.02	15.05	21.86	30.88	0.001	0.975	0.024	0.695	±0.004	3
CaMg4	60	15.7	−8.75	21.89	−9.19	30.89	31.73	22.04	15.07	21.88	30.88	0.001	0.976	0.023	0.690	±0.012	4
CaMg4	180	16.9	−8.91	21.72	−9.19	30.72	31.73	22.04	15.07	21.90	30.89	0.001	0.978	0.021			
CaMg4	1440	17.9	−8.94	21.69	−9.19	30.69	31.73	22.04	15.07	21.94	30.93	0.001	0.983	0.016	0.692	±0.023	4
CaMg4	4320	18.5	−9.53	21.09	−9.19	30.10	31.73	22.04	15.07	21.96	30.95	0.001	0.986	0.013			
CaMg4	20,160	19.4	−9.31	21.31	−9.19	30.32	31.73	22.04	15.07	21.94	30.94	0.001	0.984	0.015			
CaMg4	129,600	19.9	−9.30	21.32	−9.19	30.33	31.73	22.04	15.07	21.97	30.96	0.001	0.988	0.011	0.684	±0.013	4
CaMg4*	5	5.6	−8.30	22.35	−9.59	31.74	31.31	21.62	14.66	21.48	30.89	0.001	0.978	0.021	0.695	±0.015	2
CaMg4 (50)*	5	5.6	−8.63	22.01	−9.59	31.41	31.31	21.62	14.66	21.48	30.89	0.001	0.978	0.021	0.694	±0.006	4
CaMg4*	1440	17.1	−8.28	22.37	−9.19	31.36	31.73	22.04	15.07	21.98	30.97	0.001	0.989	0.010	0.703	±0.015	2
CaMg4 (50)*	1440	17.1	−8.81	21.83	−9.19	30.83	31.73	22.04	15.07	21.98	30.97	0.001	0.989	0.010	0.708	±0.02	1
CaMg5	5	4.6	−9.03	21.60	−9.57	30.99	31.33	21.64	14.68	21.52	30.91	0.001	0.980	0.019			
CaMg5	13	6.4	−6.90	23.80	−9.37	32.94	31.54	21.85	14.89	21.71	30.90	0.001	0.978	0.021			
CaMg5	25	8.1	−9.19	21.44	−9.20	30.46	31.72	22.03	15.06	21.88	30.89	0.001	0.977	0.022			
CaMg5	60	12.4	−9.23	21.39	−9.18	30.39	31.74	22.05	15.08	21.88	30.87	0.001	0.974	0.025			
CaMg5	180	13.0	−8.77	21.87	−9.18	30.86	31.74	22.05	15.08	21.87	30.86	0.001	0.973	0.026			
CaMg5	1440	14.2	−9.68	20.93	−9.18	29.94	31.74	22.05	15.08	21.95	30.93	0.001	0.983	0.016			
CaMg5	4320	14.8	−9.55	21.06	−9.18	30.06	31.74	22.05	15.08	21.96	30.94	0.001	0.985	0.014			
CaMg5	20,160	15.7	−9.78	20.83	−9.18	29.84	31.74	22.05	15.08	21.94	30.93	0.001	0.983	0.016			
CaMg5	129,600	16.2	−9.77	20.84	−9.18	29.85	31.74	22.05	15.08	21.97	30.96	0.001	0.987	0.012			

for #CaMg4 were chosen for this testing due to its high Mg/Ca ratio, which induces elevated metastability of ACMC (see below) and its stronger sensitivity to potential isotopic re-equilibration and/or exchange of oxygen isotopes between the solid carbonate and H_2O.

4. RESULTS

4.1. Phase transformation

The formation of ACMC can be traced by the in situ Raman spectra at wave number $1085 \pm 1\ cm^{-1}$. In Fig. 1B the transformation of ACMC into Mg calcite is documented by the evolution of the maximum intensity (I_{max}) of the v_1 vibration band of the solid CO_3^{2-}. Note that at 25 min of reaction time the mixing of the two stock solution stops. During the experiments ACMC is present up to about 26 and 35 min of reaction time for #MgCa5 and #MgCa4, respectively. Subsequently, ACMC transformed to Mg calcite and after 35 and 45 min Mg calcite is the sole solid phase, for #MgCa5 and #MgCa4, respectively. The $MgCO_3$ content of the precipitates varies from 4.6 to 19.9 mol% and is increasing as a function of reaction time (Table 1). As ACMC starts to transform, a strong net uptake of Mg ions from the solution into the precipitate occurs, which finally results in the formation of high Mg calcite with 20 and 16 mol% $MgCO_3$ for experiments #MgCa4 and #MgCa5, respectively (Table 1). The calculated solubility products of ACMC and Mg calcite achieve steady state conditions for ACMC and thermodynamic equilibrium in the case of the final Mg calcite (see #MgCa4 in Purgstaller et al., 2016). The reproducibility of the experimental protocol is assessed by the result of the experiment #CaMg4*. In this run, that was performed under identical conditions to experiment #CaMg4, the Mg content of the solid phase after 1440 min of reaction time was 17.1 $\pm$ 0.4 mol% $MgCO_3$ and in excellent agreement with the Mg content of experiment #CaMg4 (i.e. 17.9 $\pm$ 0.4 mol% $MgCO_3$) at the same reaction time (see Table 1).

4.2. Evolution of oxygen isotope distribution of the precipitate and solution

In Fig. 2A the oxygen isotopic composition of the precipitates is displayed as a function of reaction time. The $\delta^{18}O_{prec}$ (VPDB) values – analyzed as Mg calcite, but referring to ACMC and Mg calcite separated from the experimental solution – behave similar for experiments #MgCa4 and #MgCa5. The initial precipitate has a $\delta^{18}O_{prec}$ value of about −9‰, which increases strongly reaching a maximum value of about −7‰ at a reaction time of 13 min, where ACMC is the reaction product. Throughout the later stage of transformation of ACMC, the $\delta^{18}O_{prec}$ values decrease to -9.5 ± 0.2‰ in the final Mg calcite (90 days). The maximum $\delta^{18}O_{prec}$ value obtained during the formation period of ACMC is highly pronounced and clearly out of the analytical error (Fig. 2). Note here that according to the required preparation step (see methodology) all precipitates were analyzed in the form of Mg calcite to provide proper isotope analyses and data correction. To assess if an

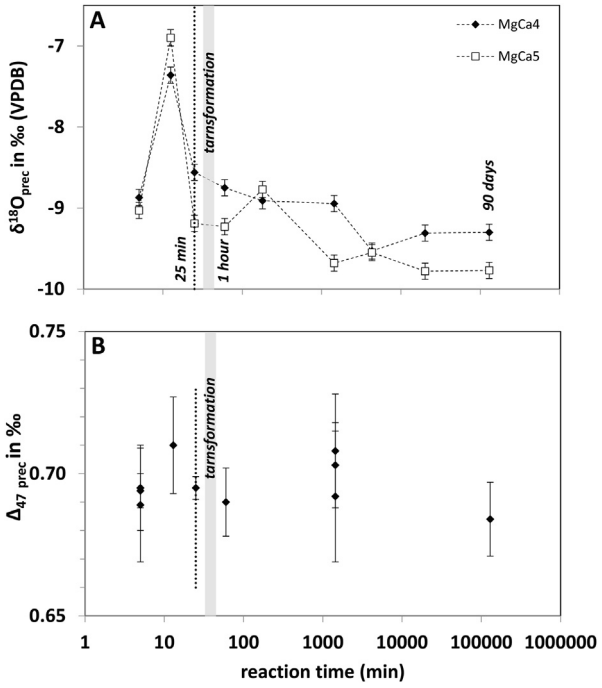

Fig. 2. Evolution of (A) measured oxygen isotope composition and (B) clumped isotope signatures of the precipitated Ca Mg carbonate (measured as Mg calcite; see methodology) as a function of reaction time during the experimental runs #MgCa4 and #MgCa5 at a given aqueous Mg/Ca ratio (see data in Table 1; clumped isotopes are only measured for experiment #MgCa4). At a reaction time of 25 min (dotted line) the continuous precipitation of amorphous calcium magnesium carbonate (ACMC) by ongoing mixing of the two stock solution ends.

oxygen isotope re-distribution between the precipitate and the H_2O included in ACMC has to be considered or not, in analogous experiments the sampled precipitates were dried separately at 25° and 50 °C (Table 1). The measured $^{18}O_{prec}$ values indicate no pronounced variability in oxygen isotope data considering their reproducibility (#CaMg4 and CaMg4*: $\delta^{18}O_{prec} = -8.6 \pm 0.2$‰, VPDB; n = 3; reaction time of 5 min, where ACMC was the reaction product).

The evolution of the $\delta^{18}O_{H2O}$ values of the experimental solution reported in Table 1 is based on the ongoing titration of the $MgCl_2$ (and NaOH) solutions into the $NaHCO_3$ reacting solution. The isotopic composition at the given experimental time for sampling was modelled by their volume fractions in the experimental solutions and individual isotopic compositions. The oxygen isotope compositions of the $MgCl_2$ and $NaHCO_3$ solution were analyzed to obtain $\delta^{18}O_{H2O} = -9.55 \pm 0.06$‰ (VSMOW; n = 5) and $= -9.80 \pm 0.07$‰ (VSMOW; n = 5). The oxygen isotope distribution of the measured initial ($NaHCO_3$) and final experimental solutions ($\delta^{18}O_{H2O} = -9.17 \pm 0.06$‰ VSMOW; n = 5) were used to estimate the isotopic composition of the added NaOH solution to be $\delta^{18}O_{H2O} = -7.5 \pm 0.1$‰ (VSMOW) by volume balancing. Accordingly, the volume balanced $\delta^{18}O_{H2O}$ values of the experimental solution at each individual reaction step were used to obtain isotope fractionation coefficients between precipitate

and solution (Table 1). Note here, that the $\delta^{18}O_{H2O} = -9.2 \pm 0.1‰$ (VSMOW) of the final experimental solution at 129.600 min (i.e. 90 days) is close to that of the $MgCl_2$ and $NaHCO_3$ solutions.

4.3. Clumped isotope data of the precipitates

The temporal evolution of the clumped isotope composition of the precipitates from the experiments is shown in Fig. 2B. Obviously, there is no systematic change of the $\Delta_{47\ prec}$ values throughout formation of ACMC and its transformation to Mg calcite. The average value of all measured data yield $\Delta_{47prec} = 0.696 \pm 0.008‰$ (n = 30), which lays within the expected range for calcite close to isotope equilibrium at 25 °C (e.g. Zaarur et al., 2013; Kele et al., 2015; Kluge et at., 2015; Hill et al., 2014; Tang et al., 2014; Tripati et al., 2015; Watkins and Hunts, 2015; Sade and Halevy, 2017: see Eq. (4) and discussion above). Thus, an impact on Δ_{47} values of Mg calcite formed via ACMC precursors compared to direct (Mg) calcite formation cannot be seen from the present and above literature data sets within the analytical uncertainty. However, considering clumped isotope values of slowest known calcite precipitation rates as found in specific speleothems ($\Delta_{47prec} = 0.660‰$; Daëron et al., 2019) the values obtained in this study for Mg calcite are higher by about $0.04 \pm 0.01‰$ and can thus be reasonably suggested that they deviate from isotopic equilibrium.

5. DISCUSSION

5.1. Oxygen isotope fractionation between Mg-bearing solids and solution

The oxygen isotope fractionation between the solid phases and the precipitating solution as a function of reaction time estimated using Eq. (3) is shown in Fig. 3 and reported in Table 1. The oxygen isotope fractionation coefficient $\alpha_{prec\text{-}water}$ ($10^3 ln\alpha_{prec\text{-}water} \approx \Delta^{18}O_{prec\text{-}water}$) follows most closely the evolution of the analyzed $\delta^{18}O_{prec}$ values in Fig. 2A. This similar pattern stems from the fact that the $\delta^{18}O_{H2O}$ values are quasi constant during the experimental runs ($-9.6 < \delta^{18}O_{H2O} < -9.2‰$, VSMOW; Table 1). Accordingly, the $10^3 ln\alpha_{prec\text{-}water}$ value reaches a maximum of about +33‰ in the amorphous precipitate at 13 min of reaction time, when ACMC is formed in the experiments. This value is significantly higher compared to that at isotope equilibrium between calcite and solution ($10^3 ln\alpha_{calcite\text{-}H2O} = 29.8‰$ at 25 °C; Coplen, 2007; Daëron et al., 2019). The obtained results suggest that the precipitates in experiments #CaMg4 and #CaMg5 discriminate ^{16}O much stronger than ^{18}O (about 3.2‰) compared to the isotope fractionation expected for calcite at isotopic equilibrium. However, subsequently to the ACMC transformation stage oxygen isotope equilibrium is approached rapidly between Mg calcite and water ($30.3 \pm 0.4‰$; Table 1). The obtained $10^3 ln\alpha_{prec\text{-}water}$ values can clearly be separated from oxygen isotope equilibrium between aragonite and H_2O, but are slightly higher for #CaMg4 (~0.5‰) or identical within the analytical error for #CaMg5 compared to that expected for calcite and H_2O at oxygen isotope equilibrium (Fig. 3). The higher $10^3 ln\alpha_{prec\text{-}water}$ values at the elevated Mg/Ca ratio in #CaMg4 can be likely explained by the incorporation of Mg in calcite. Indeed, Mavromatis et al. (2012) showed that higher $MgCO_3$ contents in calcite yield in higher $\alpha_{Mg\text{-}calcite\text{-}water}$ values. This relationship is documented by $10^3 ln\alpha_{prec\text{-}water}$ values of 29.85‰ and 30.33‰ for 16.2 and 19.9 mol% $MgCO_3$ in experiments #CaMg5 and #CaMg4, respectively. The difference of about 0.5‰ is similar to that reported by Mavromatis et al. (2012) for Mg calcites (i.e. 0.6‰) with similar Mg contents to that of this study and is in general agreement with slightly higher $^{18}\alpha$ values caused by denser structures and by stronger chemical bonds for Mg rich carbonate minerals (e.g. Mg calcite: Tarutani et al., 1969; dolomite: Horita, 2014).

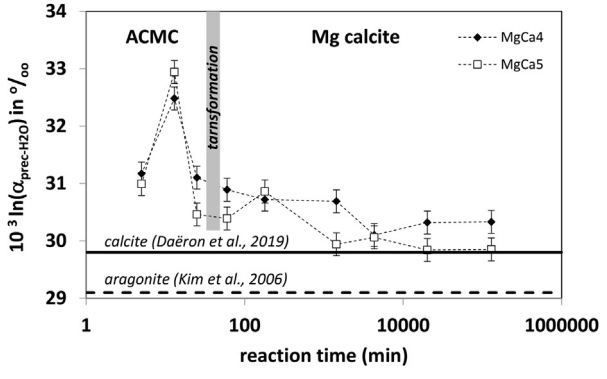

Fig. 3. Apparent oxygen isotope fractionation between the precipitated Ca Mg carbonate and water ($\alpha_{prec\text{-}water} = (^{18}O/^{16}O)_{prec}/(^{18}O/^{16}O)_{water}$) in the present study during the experimental runs #MgCa4 and #MgCa5 (see data in Table 1) versus the oxygen isotope fractionation between calcite/aragonite and water at equilibrium at 25 °C obtained from literature (solid/dashed line, respectively). The shaded area marks the transformation period of ACMC to Mg calcite in both experiments.

In earlier studies deviation from oxygen isotope equilibrium between calcite and water results in smaller fractionation coefficients ($\alpha_{calcite\text{-}water}$), which are e.g. kinetically driven by non-isotope equilibrated DIC (e.g. Dietzel et al., 2009; Watkins et al., 2014). In the present study, the DIC species of the initial experimental $NaHCO_3$ solution are at isotopic equilibrium with H_2O with respect to oxygen isotopes (see above), thus the analyzed H_2O oxygen isotope composition determines DIC species compositions. Accordingly, in Fig. 4A the oxygen isotope composition of the individual DIC species, $CO_{2(aq)}$, HCO_3^- and CO_3^{2-} can be estimated using the oxygen isotope fractionation coefficients (α) between H_2O and DIC species at isotope equilibrium (see $\alpha_{CO2(aq)\text{-}water}$, $\alpha_{HCO3\text{-}\ \text{-}water}$ and $\alpha_{CO32\text{-}\ \text{-}water}$ values at 25 °C in Table 2). The estimated range of $\delta^{18}O$ values for DIC species reflects the variability of the isotopic composition of H_2O, where $\delta^{18}O$ of DIC represents the obtained value for total DIC, which was calculated by the relative molar fractions of the aqueous DIC species and their individual oxygen isotopic compositions (see Table 1). Following this approach the ^{16}O enrichment in the ACMC at 13 min of reaction time cannot be explained by equilibrium conditions between calcite and solution (see open symbol

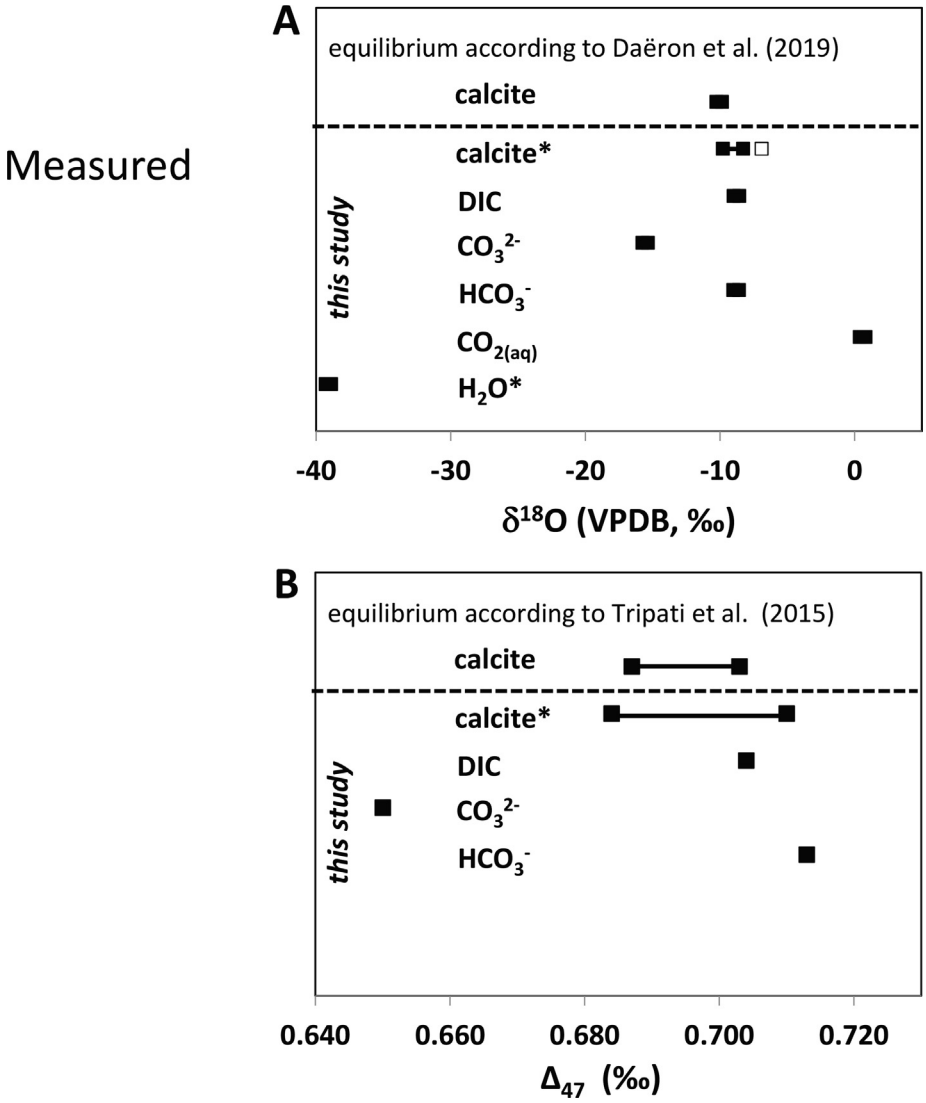

Fig. 4. Range of oxygen isotope (A) and clumped isotope values (B) of the Ca-Mg carbonate precipitates from experiments #MgCa4 and #MgCa5 as well as individual isotope values of calcite and DIC species calculated using fractionation coefficients from literature displayed in Table 2 at pH 8.3 and 25 °C considering isotope equilibrium conditions (see values in Table 1). In (A) the open symbol denotes the heaviest measured oxygen isotope value of the precipitate at a reaction time of 13 min (see Fig. 2). Dashed lines separate calculated isotope values of calcite (above) from measured values of the present study for H_2O (H_2O*) and calcite (calcite*) and estimated values for DIC species (all below). calcite* range includes data, where ACMC and Mg calcite is precipitated in the experiments. □: value at 13 min reaction time where ACMC is formed.

Table 2
Oxygen isotope fractionation factors (α) between water (H_2O) and DIC species as well as between calcite/aragonite and H_2O approaching isotope equilibrium from literature at 25 °C.

I – ii	$\alpha(^{18}O/^{16}O)_{i\text{-}ii}$	$10^3\ln(\alpha_{i\text{-}ii})$
$CO_{2(aq)}$ – water[#1]	1.04130	40.47
HCO_3^- – water[#1]	1.03152	31.03
CO_3^{2-} – water[#1]	1.02448	24.19
calcite – water[#2]	1.03025	29.76
aragonite – water[#3]	1.02953	29.10

[#1] Beck (2005).
[#2] Daëron et al. (2019).
[#3] Kim et al. (2006).

versus equilibrium value in Fig. 4A). In contrast the observed highest $10^3\ln(\alpha_{prec\text{-}water})$ of about 33‰ at 13 min can be assigned to the rapid incorporation of DIC species during instantaneous ACMC formation without isotopic re-equilibration. For instance, CO_3^{2-} in the ACMC precipitate is gained from deprotonation of HCO_3^- (dominant at pH 8.3) without isotopic re-equilibration with H_2O (Fig. 4A). In this approach the precipitate shifts to isotopically heavier values as HCO_3^- is isotopically heavier than CO_3^{2-} (see Fig. 4A). However, the highest $\delta^{18}O_{prec}$ values (open symbol in Fig. 4A) cannot be explained by this approach considering solely HCO_3^-, instead they may be caused by the rapid incorporation of CO_3^{2-} gained from

additionally occurring aqueous complexes in such highly concentrated experimental solutions.

In Table A1 (Appendix) the distribution of aqueous species of the experimental solutions are provided. The highest concentrations in respect to carbonate-bearing aqueous complexes are obtained in the decreasing order of $MgHCO_3^+$, $MgCO_3°$, $CaHCO_3^+$ and $CaCO_3°$. Interestingly, the concentrations of magnesium carbonate aqueous complexes show a maximum value at a reaction time of 13 min (Fig. 5A), where the Mg and DIC concentration is at highest level (see Table A1). The maximum concentration of the aqueous $MgHCO_3^+$ and $MgCO_3°$ species coincides with the maximum of the oxygen isotope fractionation between solid phase and solution displayed in Fig. 3. The co-variation of the two parameters is better displayed by plotting the concentration of $MgHCO_3^+$ and $MgCO_3°$ as a function of $10^3\ln(\alpha_{prec\text{-}water})$ value (Fig. 5B), where the shaded area is referred to the occurrence of solely amorphous calcium magnesium carbonate (ACMC) as precipitate. The formation of ACMC is accompanied by a highly dynamic exchange of ions with the forming solution (e.g. Mavromatis et al, 2017a; Purgstaller et al., 2017; Prus et al., 2019), thus the strong relationship between

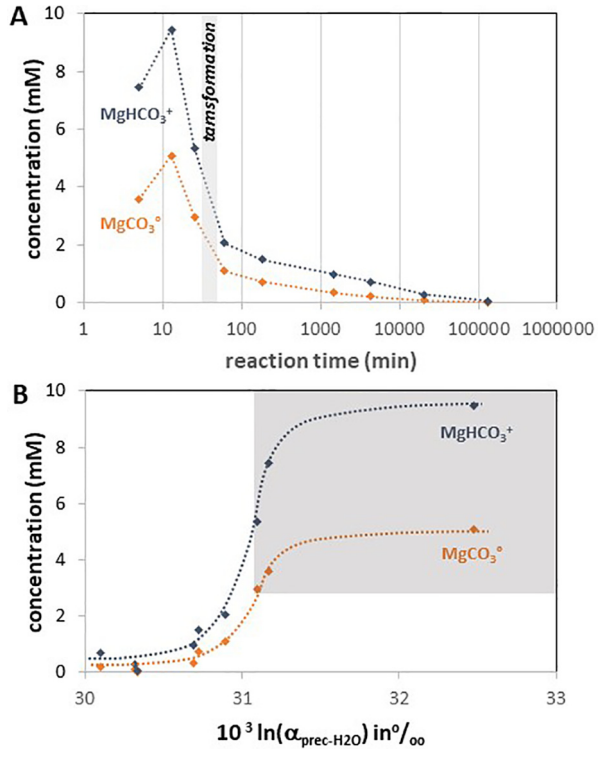

Fig. 5. The concentration of the Mg (bi)carbonate aqueous complexes, exemplarily shown for experimental run #MgCa4 as a function of reaction time (A) and apparent oxygen isotope fractionation between Ca Mg carbonate precipitate and water (B). Note here, that the highest concentration of Mg (bi)carbonate aqueous complexes at about 13 min in (A) corresponds to the maximum of oxygen isotope fractionation observed in Fig. 3. The shaded area in (B) is referred to the occurrence of solely amorphous calcium magnesium carbonate (ACMC) as precipitate in the experiment.

$[MgHCO_3^+] + [MgCO_3°]$ and $10^3\ln(\alpha_{prec\text{-}water})$ hints on the impact of both aqueous complexes on the isotopically heavy ACMC. This highly dynamic ion exchange mechanism is in accordance with the general perception about amorphous carbonate phases of Jensen et al. (2018), who concluded based on neutron and X-ray total scattering in combination with molecular modeling that the local arrangement of the ions in amorphous calcium carbonate are more similar to those ions in aqueous solution than to any of the $CaCO_3$ minerals. Following this approach, $MgHCO_3^+$ and/or $MgCO_3°$ have to be isotopically enriched in ^{18}O. This isotopic enrichment can be explained by the assumption of Uchikawa and Zeebe (2013), who postulated that magnesium carbonate aqueous complexes, such as $MgCO_3°$, are enriched in the ^{18}O compared to dissolved carbonate in accordance to their distribution of stable carbon isotopes. However, from their experimental data set no discernible effect of Mg^{2+} ions on the oxygen isotope fractionation in the CO_2–H_2O system could be observed in reactive solutions with up to 2.5 mM of Mg. In the experiments of this study the Mg concentration of the precipitating solution is up to 10 times higher and thus the impact of magnesium carbonate aqueous complex on oxygen isotope distribution might be much more pronounced. In any case, distinct oxygen isotope fractionation factors between Mg (bi)carbonate aqueous complexes and H_2O cannot be accurately estimated by the present study as more isotope data is needed at different pH, Mg and DIC contents.

The above proposed model of magnesium calcium carbonate precipitation corresponds with the conceptual model for crystalline $CaCO_3$ formation, where at low precipitation rates $CaCO_3$ is formed exclusively from aqueous CO_3^{2-} ions (e.g. Devriendt et al., 2017). At high precipitation rates partly HCO_3^- (or other bearing (bi)carbonate complexes) might be incorporated in the precipitate (see Watkins et al., 2014). However, the composition of ACMC, its solubility behaviour (see details in Purgstaller et al., 2019) and its structural composition (e.g. Nebel et al., 2008) hint on almost exclusively the CO_3^{2-} ion to be incorporated into the solid phase. As such, it can be reasonably assumed that the uptake of CO_3^{2-} ions from the solution during ACMC formation induces an instantaneous chemical response by rapid formation of aqueous CO_3^{2-} from DIC species, e.g. HCO_3^- and $MgHCO_3^+$ and $MgCO_3°$ species. Chemical re-equilibration is fast, but significant longer time is required to reach oxygen isotopic re-equilibration. Thus, the chemically incorporated CO_3^{2-} in the precipitate has partly the oxygen isotope composition of the dissolved (bi)carbonate-bearing species. As a function of reaction time CO_3^{2-} in ACMC starts to isotopically exchange with the solution, finally approaching isotope equilibrium conditions (see Fig. 3). This highly dynamic exchange behavior of ACMC with the solution can be followed by obtaining a maximum $\delta^{18}O_{prec}$ value, which is explained by the interim presence of isotopically heavy $MgHCO_3^+$ and $MgCO_3°$ species (Fig. 5). This dynamic exchange approach confirms the chemical concept of Mg content and Mg isotopes in ACMC to be regulated by the current Mg/Ca ratio and Mg isotope composition of the precipitating solution (e.g. Blue and Dove, 2015, Mavromatis et al., 2017a; Purgstaller et al.,

2016, 2019). These findings support the highly dynamic coupled dissolution-reprecipitation mechanisms of ACMC transformation to Mg calcite instead of solid state transformation mechanism.

In our study, the formation of ACMC occurs after the addition of the $(Ca,Mg)Cl_2$ solution to the $NaHCO_3$ solution. Note here that initially the $NaHCO_3$ solution is isotopically equilibrated with respect to oxygen isotopes. After mixing of the two solutions instantaneous precipitation of ACMC occurs, but also $MgHCO_3^+$ and $MgCO_3°$ aqueous complexes form in the aqueous phase. These complexes are likely isotopically heavier compared to the free CO_3^{2-} (aq) as discussed above. The 25 min of reaction time at the onset of each run during which the $(Ca,Mg)Cl_2$ solution was titrated into the reactor is a rather short time for complete oxygen isotope re-equilibration between re-distributed DIC species at the present conditions (e.g. Weise and Kluge, 2019). Thus, the absolute value of the oxygen isotope composition of $MgHCO_3^+$ and $MgCO_3°$ species in the present case cannot be predicted from the analyzed isotope range of the precipitates that exhibit changes of about 1.5‰ between 5 and 25 min of reaction time (see Figs. 2A and 5B). Nonetheless, the relationship between their occurrences and more positive $10^3\ln(\alpha_{prec\text{-}water})$ values is clearly indicating their relatively heavy oxygen isotope composition by considering the highly dynamic exchange of ions between ACMC and the precipitating solution (see below).

The calcite formed via ACMC in this study exhibits oxygen isotope ratios more positive than expected for calcite under equilibrium conditions (i.e. Daëron et al., 2019). The uncommon oxygen isotope composition of the amorphous precursor phases can be assigned to kinetic processes related to the instantaneous trapping of the oxygen isotopic composition from DIC species at the initial stage of ACMC formation. This observation comes in contrast to isotopically lighter calcite growing at fast rates under the classical nucleation-growth model where oversaturation of the fluid with respect to the forming calcite is comparatively low (see Dietzel et al., 2009). In this case, the growth rate effect can be explained by surface entrapment of CO_3^{2-} from the solution at the growing calcite, which differs in its oxygen isotope distribution compared to the aqueous CO_3^{2-}. In this case a partial isotope re-equilibrating process prior to calcite overgrowth is expected and its extent is a function of mineral growth rate. This kinetically driven oxygen isotope fractionation effect between calcite and aqueous CO_3^{2-} at the mineral-water interface is not valid during ACMC precipitation, due to instantaneous ion exchange between the bulk ACMC and aqueous solution. Thus, ACMC can be considered to behave similar to a separate liquid medium (Jensen et al., 2018, Leukel et al., 2018) with a given bulk ion and oxygen isotope exchange and fractionation behavior in respect to the aqueous fluid phase (see also Purgstaller et al., 2019).

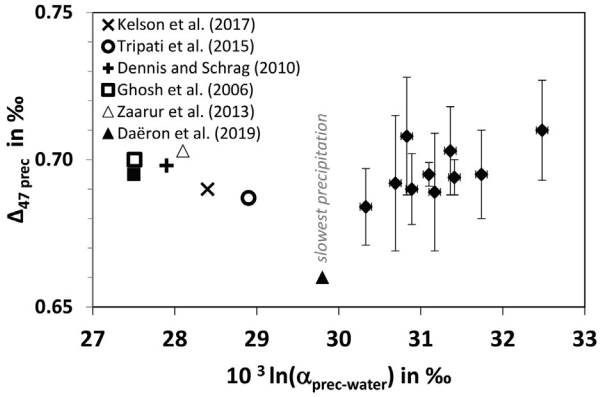

Fig. 6. Clumped isotope data versus oxygen isotope fractionation data for precipitation experiment #MgCa4 (◆: this study; Table 1). Data from Dennis and Schrag (2010), Ghosh et al. (2006) and Zaarur et al. (2013) are given in respect to clumped isotope values as refitted according to Tripati et al. (2015) and are based on calcite precipitation experiments. Kelson et al. (2017) reports carbonate clumped isotope calibration from calcite synthesis. Values from Kluge et al. (2015) are based on clumped isotope calibration and oxygen isotope data of calcite. The isotope data from Daëron et al. (2019) are from very slow precipitating calcite found in speleothems, thus most likely approaching isotopic equilibrium.

5.2. Clumped isotopes of Mg calcites from ACMC transformation

The clumped isotope composition of the precipitates in the present experiments shows no systematic change during the formation of ACMC and its transformation to Mg calcite (Fig. 2). The measured Δ_{47} values indicate no impact of experimental Mg calcite formation pathway via (i) amorphous precursor and (ii) direct precipitation (see Fig. 6). But former and Δ_{47} values obtained in this study are still not representing isotopic equilibrium (see Daëron et al., 2019). No significant correlation could be observed between clumped isotope and oxygen isotope fractionation behavior from our experiments (Fig. 6; Tables 1 and A1). The absence of correlation indicates that – in contrast to oxygen isotopes – the Δ_{47} distribution of distinct DIC species is not affecting the clumped isotope composition of the precipitates in the present experiments. As even instantaneous uptake of carbonate species in ACMC does not affect the clumped isotopic composition of the final Mg calcite, Δ_{47} distribution in Mg calcite seems to behave conservatively in respect to tracing its formation conditions at the given experimental conditions (25 °C, pH 8.3). This conservative behavior is consistent with no significant dependence of Δ_{47} values on growth rate of $CaCO_3$ reported by Tang et al. (2014), Kluge et al. (2015), and Levitt et al. (2018); even for carbonate bearing apatite (Stolper and Eiler, 2015). However, note here that pH was found to play a role in influencing Δ_{47} values. At strong alkaline conditions Δ_{47} values could be affected during carbonate formation by kinetic isotope effects based on non-complete isotopic re-equilibration of DIC species (Hill et al., 2014; Tang et al., 2014).

Considering Δ_{47} values of carbonate minerals close to isotope equilibrium, Bonifacie et al. (2017) postulated an universal calibration for all (Ca, Mg, Fe)CO_3 minerals to be valid with no measurable effect due to cation ordering. In contrast, recently it was shown that a carbonate

mineral-specific clumped isotope fractionation has to be considered for different minerals (Müller et al., 2019; Bernasconi et al., 2019). The clumped isotope values obtained for (Mg) calcite in this study lay within the range documented for (Mg) calcite in the literature (Fig. 6 and discussion above), with exception of the lowest precipitation rates observed in speleothems. This observation confirms that most natural and synthetic carbonate mineral formation is out of equilibrium.

6. IMPLICATIONS FOR THE USE OF OXYGEN AND CLUMPED ISOTOPE DATA OF MG CALCITE AS ENVIRONMENTAL PROXY

The (trans)formation of amorphous to crystalline carbonate, such as Mg calcite, may have to be considered in carbonate archives due to the observed geochemical offsets compared to the direct precipitation of Mg calcite (e.g. Immenhauser et al., 2016). The variability of $\delta^{18}O_{prec}$ values in the present experiments clearly shows that the use of the finally obtained reaction product, Mg calcite, is challenging for temperature reconstruction without premises. Thus, Mg calcite formation via amorphous precursors has to be considered in addition to other well-known effects on oxygen isotope fractionation, e.g. metabolic processes of a host organism, differential composition of the precipitating fluid from the bulk environmental fluid, precipitation rate, mineral composition and structure, and ionic strength (e.g. Spero and Lea, 1996; Owen et al., 2002). From our experimental results the following scenarios for potential impact of the formation pathway from ACMC to Mg calcite to the variability of oxygen isotope composition of Mg calcite are developed depending on the distinct transformation settings.

Scenarios in carbonate precipitating surroundings comprise of ACMC to be (i) transformed to Mg calcite at the same aqueous surrounding and physicochemical conditions of its formation, (ii) removed from its precipitation environment with subsequent transformation in the absence of an aqueous solution, and (iii) removed from its precipitation environment and a subsequent transformation within an aqueous surrounding at physicochemical conditions different from its formation environment. In scenario (i) our data show that the oxygen isotope composition of the final Mg calcite is approaching isotope equilibrium conditions, thus Mg calcite can be used for e.g. temperature reconstruction, although it is formed via an ACMC precursor. In contrast, scenario (ii) yield in the separation of the amorphous precipitate, which can be significantly enriched in ^{18}O of the CO_3^{2-} ions compared to isotope equilibrium conditions. This isotopically heavier oxygen isotope signal is subsequently carried in the final Mg calcite if no water is present for re-equilibration (see Fig. 2A). A $\delta^{18}O_{calcite}$ value of 3‰ higher than that expected at isotopic equilibrium at 25 °C corresponds to a temperature offset of about −12 °C according to Coplen (2007) and Daëron et al. (2019) equations. In this second scenario the oxygen isotope exchange between the liberated H_2O gained from decomposition of amorphous carbonate and the finally formed calcite likely has no significant effect on the final (Mg) calcite in the present experimental approach as our results show no pronounced variability of oxygen isotope data of ACMC transformation to Mg calcite by distinct drying procedures (#CaMg4 and CaMg4* in Table 1). However, assessment of this effect is complicated by the still unknown (i) isotope fractionation between H_2O from the bulk solution and the amorphous phase and (ii) exchange dynamics of liberated H_2O and the CO_3^{2-}. Scenario (iii) is in particular challenging to re-construct formation temperatures of (Mg) calcite from $\delta^{18}O_{calcite}$ value as the distinct aqueous transformation environment may be different in respect to oxygen isotope composition of the solution as well as $CaCO_3$ precipitation rate, temperature etc. of transformation compared to ACMC formation conditions. Thus, in the third scenario the oxygen isotope composition of the final Mg calcite can be reasonably suggested to be highly influenced by the transformation conditions, documented by the previously discussed highly dynamic ion exchange behavior of ACMC throughout its (trans)formation to Mg calcite. Assessing the extent of oxygen isotope (and also elemental) exchange and re-equilibration for distinct highly variable (trans)formation settings requires additional data sets on exchange reaction kinetics and on the individual transformation settings.

The evolution of Δ_{47} values of Mg calcite in this study indicates no direct impact of experimental Mg calcite formation by amorphous precursor or direct precipitation (see Fig. 6). However, the measured Δ_{47} values are distinct from isotopic equilibrium conditions as suggested by Daëron et al. (2019). According to its constancy during the mineralogical evolution, Δ_{47} can be considered as a rather conservative proxy compared to oxygen isotope signatures. In contrast to oxygen isotopes, the clumped isotopes of the precipitates seem to be unchanged during the formation of ACMC and its subsequent transformation to Mg calcite for both scenarios (i) and (ii) (see Figs. 2B and 6). For scenario (iii) a change of aqueous solution composition considering non-equilibrated DIC to change the clumped isotope signature due to the highly dynamic ion exchange behavior of ACMC with the aqueous solution is consequently expected, however, straightforward outcomes cannot be proposed and have to be investigated in further experimental approaches. In addition, temperature changes during transformation of ACMC may affect the Δ_{47} of the final Mg calcite. Note, that an impact of Δ_{47} values on carbonate mineral precipitates pointed e.g. to vital effect on $CaCO_3$ cannot be ruled out (e.g. Kimball et al., 2016; Spooner et al., 2016), but are suggested to be mostly relevant for non-equilibrated DIC, in particular at elevated pH and/or strong CO_2 exchange of the aqueous solution with the atmosphere; commonly associated with kinetics of CO_2 hydration/hydroxylation reactions (e.g. Katz et al., 2017).

Combining data sets of oxygen isotope and clumped isotope signatures of carbonates are highly promising to reconstruct, e.g. Mg calcite formation environments. For instance, mineral formation temperature can be reconstructed from clumped isotope data and subsequently the oxygen isotope composition of the precipitating solution can be revealed by the traditional oxygen isotope values

using the obtained temperature, where solution isotopic composition hints on its provenance, evaporation degree etc. (e.g. Boch et al., 2019). However, for this approach, isotope equilibrium conditions have to be approached, which may not be necessarily the case considering ACMC precursor pathways, in particular for oxygen isotope distribution in Mg calcite.

In consequence, experiments on the clumped and oxygen isotope exchange behavior during ACMC formation and its transformation at environments differing from its initial formation conditions (regarding T and isotopic composition of the transformation solution, see scenario III) are highly demanded. Recent aragonite to calcite transformation experiments by Guo et a. (2019) reveal the latter to be a crucial approach also for transformation of crystalline carbonate minerals indicating that the temperatures signal recorded by clumped isotopes in the primary aragonite can be preserved in the replacement calcite. Thus, one main focus for further research has to be given on the influence of temperature changes during the transformation of ACMC on $\Delta_{47}/\delta^{18}O$ values of the final Mg calcites and on the effect of pH (see also Tripati et al., 2015).

7. SUMMARY AND CONCLUSIONS

The oxygen isotopic composition of the precipitates obtained from experiments, where Mg calcite forms via the transformation of an ACMC precursor, shows higher oxygen isotope fractionation between precipitate and water compared to those expected at isotopic equilibrium conditions for (Mg) calcite, in particular at the initial stage of ACMC formation. In contrast to oxygen isotopes, the clumped isotopes of the precipitates are constant during the experimental runs. From the experimental results the following main conclusions can be drawn:

(i) The present experiments indicate that the $\delta^{18}O$ values of the Mg calcite that formed via ACMC are highly variable caused by kinetic effects related to the instantaneous trapping of the isotopic composition from DIC species at the initial stage of ACMC formation (e.g. CO_3^{2-}, HCO_3^-, $MgCO_3°$, and $MgHCO_3^+$). This effect causes higher apparent oxygen isotope fractionation coefficients than expected at isotope equilibrium between (Mg) calcite and solution. Throughout the ongoing formation of Mg calcite oxygen isotope equilibrium is almost approached between Mg calcite and water.

(ii) From ACMC (trans)formation experiments a highly dynamic exchange reaction between ions/isotopes in the amorphous phase (ACMC) and the solution is postulated.

(iii) Oxygen isotope composition of Mg calcite formed via ACMC can be highly affected by its (trans)formation pathway, which is validated by three scenarios based on open to closed conditions in respect to the transformation solution (I and II) and on the transformation environment/conditions being different from that where ACMC formed (III).

(iv) Clumped isotopes of Mg calcite seem to be more promising than oxygen isotopes to be used as temperature proxy even at fast precipitation conditions, where ACMC precursors occur, but in particular scenario III has still to be investigated for this scope.

(v) In a recent study Daëron et al. (2019) suggested based on isotope data of very slow forming calcite that the majority of (Mg) calcites precipitated at Earth's surface does not reach oxygen isotope equilibrium as it precipitates in general too fast. In contrast our results indicate that very rapidly forming Mg calcite via amorphous precursor at highest precipitation rates is nearly approaching oxygen isotope equilibrium after a certain transformation time. This contrasting outcome might be explained by high reaction dynamics of ion and isotope exchange according to conclusion (ii).

Declaration of Competing Interest

The authors declare that they have no known competing financial interests or personal relationships that could have appeared to influence the work reported in this paper.

ACKNOWLEDGEMENT

The authors highly appreciate support for sample preparation as well as solid and liquid analyses by Judith Jernej and Andrea Wolf at NAWI Graz Central Lab for Water, Minerals and Rocks. This work was financially supported by Marie Skłodowska-Curie and by the FWF-DFG project Charon II (FWF-I3028-N29). Clumped isotope analyses at Heidelberg were done using an IRMS instrument that was funded through the grant DFG-INST 35/1270-1. T.K. acknowledges funding by the Heidelberg Graduate School of Fundamental Physics (HGSFP) and is grateful for technical help provided by the team 'physics of environmental archives' to maintain the IRMS instrument. The authors greatly appreciate the handling of the manuscript by Claire Rollion-Bard and the constructive comments of Rinat Gabitov and an additional anonymous reviewer.

APPENDIX

See Table A1.

Table A1
Distribution of aqueous species calculated by measured concentrations in reactive solution and PHPREQ C modelling approach (see Purgstaller et al., 2016 for details). Concentrations are given in mmol L^{-1}. *separate analogous experiment.

	Time min	CO_2	HCO_3^-	CO_3^{2-}	DIC	Mg^{2+}	Ca^{2+}	$MgCO_3°$	$MgHCO_3^+$	$CaCO_3°$	$CaHCO_3^+$
CaMg4	5	0.52	515.91	9.89	526.32	14.97	3.69	3.59	7.45	1.10	1.96
CaMg4	13	0.28	279.44	6.35	286.07	24.42	3.84	5.08	9.46	1.06	1.71
CaMg4	25	0.09	86.10	2.10	88.29	27.23	6.18	2.98	5.35	1.05	1.64
CaMg4	60	0.07	74.12	1.78	75.97	12.06	0.39	1.10	2.07	0.06	0.09
CaMg4	180	0.07	69.40	1.51	70.98	8.89	0.20	0.73	1.49	0.03	0.05
CaMg4	1440	0.07	65.29	1.04	66.40	6.08	0.14	0.35	0.99	0.01	0.03
CaMg4	4320	0.07	66.35	0.86	67.28	4.32	0.13	0.21	0.72	0.01	0.03
CaMg4	20,160	0.06	58.43	0.87	59.36	1.89	0.16	0.09	0.28	0.01	0.03
CaMg4	129,600	0.06	59.30	0.67	60.03	0.47	0.17	0.02	0.07	0.01	0.04
CaMg4*	5	0.54	538.86	11.82	551.22	14.03	1.05	3.44	6.80	0.32	0.55
CaMg4(50)*	5	0.54	538.86	11.82	551.22	14.03	1.05	3.44	6.80	0.32	0.55
CaMg4*	1440	0.09	86.14	0.88	87.11	8.17	0.11	0.59	1.93	0.01	0.04
CaMg4(50)*	1440	0.09	86.14	0.88	87.11	8.17	0.11	0.59	1.93	0.01	0.04
CaMg5	5	0.52	517.01	9.91	527.44	11.55	0.425	2.77	5.75	0.13	0.23
CaMg5	13	0.30	296.85	6.40	303.55	18.42	0.524	3.79	7.40	0.14	0.24
CaMg5	25	0.10	97.42	2.17	99.69	21.87	0.666	2.40	4.72	0.11	0.19
CaMg5	60	0.09	86.79	2.20	89.08	11.38	0.387	1.27	2.22	0.07	0.10
CaMg5	180	0.08	84.68	2.30	87.06	9.79	0.390	1.14	1.86	0.07	0.10
CaMg5	1440	0.09	86.20	1.38	87.67	6.79	0.137	0.50	1.37	0.02	0.04
CaMg5	4320	0.08	81.83	1.18	83.09	5.15	0.182	0.32	1.01	0.02	0.05
CaMg5	20,160	0.08	76.91	1.27	78.26	2.77	0.183	0.19	0.51	0.02	0.05
CaMg5	129,600	0.08	77.28	0.95	78.31	1.38	0.189	0.07	0.26	0.02	0.05

APPENDIX A. SUPPLEMENTARY MATERIAL

Supplementary data to this article can be found online at https://doi.org/10.1016/j.gca.2020.02.032.

REFERENCES

Adkins J. F., Boyle E. A., Curry W. B. and Lutringer A. (2003) Stable isotopes in deep-sea corals and a new mechanism for "vital effects". *Geochim. Cosmochim. Acta* **67**, 1129–1143.

Albéric M., Bertinetti L., Zou Z., Fratzl P., Habraken W. and Politi Y. (2018) The crystallization of amorphous calcium carbonate is kinetically governed by ion impurities and water. *Adv. Sci.* **5**, 1701000.

Bajnai D., Fiebig J., Tomašových A., Milner Garcia S., Rollion-Bard C., Raddatz J., Löffler N., Primo-Ramos C. and Brand U. (2018) Assessing kinetic fractionation in brachiopod calcite using clumped isotopes. *Sci. Rep.* **8**, 533.

Beck W. C., Grossman E. L. and Morse J. W. (2005) Experimental studies of oxygen isotope fractionation in the carbonic acid system at 15°C, 25°C, and 40°C. *Geochim. Cosmochim. Acta* **69**, 3493–3503.

Bernasconi S., van Dijk J., Müller I. and Fernandez A. (2019) Is there a universal clumped isotope temperature calibration for all carbonate minerals?. *Goldschmidt Abstr.* **267**.

Blue C. R. and Dove P. M. (2015) Chemical controls on the magnesium content of amorphous calcium carbonate. *Geochim. Cosmochim. Acta* **148**, 23–33.

Boch R., Wang X., Kluge T., Leis A., Lin K., Pluch H., Mittermayr F., Baldermann A., Böttcher M. E. and Dietzel M. (2019) Aragonite–calcite veins of the 'Erzberg' iron ore deposit (Austria): environmental implications from young fractures. *Sedimentology* **66**, 604–635.

Bonifacie M., Calmels D., Eiler J. M., Horita J., Chaduteau C., Vasconcelos C., Agrinier P., Katz A., Passey B. H., Ferry J. M. and Bourrand J.-J. (2017) Calibration of the dolomite clumped isotope thermometer from 25 to 350°C, and implications for a universal calibration for all (Ca, Mg, Fe)CO_3 carbonates. *Geochim. Cosmochim. Acta* **200**, 255–279.

Burgener L. K., Huntington K. W., Sletten R., Watkins J. M., Quade J. and Hallet B. (2018) Clumped isotope constraints on equilibrium carbonate formation and kinetic isotope effects in freezing soils. *Geochim. Cosmochim. Acta* **235**, 402–430.

Carino A., Testino A., Andalibi M. R., Pilger F., Bowen P. and Ludwig C. (2017) Thermodynamic-kinetic precipitation modeling. A case study: the amorphous calcium carbonate (ACC) precipitation pathway unravelled. *Cryst. Growth Des.* **17**, 2006–2015.

Coplen T. B. (2007) Calibration of the calcite-water oxygen-isotope geothermometer at Devils Hole, Nevada, a natural laboratory. *Geochim. Cosmochim. Acta* **71**, 3948–3957.

Daëron M., Blamart D., Peral M. and Affek H. P. (2016) Absolute isotopic abundance ratios and the accuracy of Δ47 measurements. *Chem. Geol.* **442**, 83–96.

Daëron M., Drysdale R. N., Peral M., Huyghe D., Blamart D., Coplen T. B., Lartaud F. and Zanchetta G. (2019) Most Earth-surface calcites precipitate out of isotopic equilibrium. *Nat. Commun.* **10**, 429.

Defliese W. F. and Lohmann K. C. (2016) Evaluation of meteoric calcite cements as a proxy material for mass-47 clumped isotope thermometry. *Geochim. Cosmochim. Acta* **173**, 126–141.

Demény A., Németh P., Czuppon G., Leél-Ossy S., Szabó M., Judik K., Németh T. and Stieber J. (2016) Formation of amorphous calcium carbonate in caves and its implications for speleothem research. *Sci. Rep.* **6**, 39602.

Dennis K. J. and Schrag D. P. (2010) Clumped isotope thermometry of carbonatites as an indicator of diagenetic alteration. *Geochim. Cosmochim. Acta* **74**, 4110–4122.

Devriendt L. S., Watkins J. M. and McGregor H. V. (2017) Oxygen isotope fractionation in the $CaCO_3$-DIC-H_2O system. *Geochim. Cosmochim. Acta* **214**, 115–142.

Dietzel M., Schön F., Heinrichs J., Deditius A. P. and Leis A. (2016) Tracing formation and durability of calcite in a Punic-Roman cistern mortar (Pantelleria Island, Italy). *Isot. Environ. Health Stud.* **52**, 112–127.

Dietzel M., Tang J., Leis A. and Köhler S. J. (2009) Oxygen isotopic fractionation during inorganic calcite precipitation – effects of temperature, precipitation rate and pH. *Chem. Geol.* **268**, 107–115.

Dietzel M., Usdowski E. and Hoefs J. (1992) Chemical and$^{13}C/^{12}$-C-and $^{18}O/^{16}$O-isotope evolution of alkaline drainage waters and the precipitation of calcite. *Appl. Geochem.* **7**, 177–184.

Eiler J. M. (2007) "Clumped-isotope" geochemistry – the study of naturally-occurring, multiply-substituted isotopologues. *Earth Planet. Sci. Lett.* **262**, 309–327.

Epstein S., Buchsbaum R., Lowenstam H. and Urey H. C. (1953) Revised carbonate-water isotopic temperature scale. *Bull. Geol. Soc. Am.* **64**.

Falk E. S., Guo W., Paukert A. N., Matter J. M., Mervine E. M. and Kelemen P. B. (2016) Controls on the stable isotope compositions of travertine from hyperalkaline springs in Oman: insights from clumped isotope measurements. *Geochim. Cosmochim. Acta* **192**, 1–28.

Fohlmeister J., Arps J., Spötl C., Schröder-Ritzrau A., Plessen B., Günter C., Frank N. and Trüssel M. (2018) Carbon and oxygen isotope fractionation in the water-calcite-aragonite system. *Geochim. Cosmochim. Acta* **235**, 127–139.

Geisler T., Perdikouri C., Kasioptas A. and Dietzel M. (2012) Real-time monitoring of the overall exchange of oxygen isotopes between aqueous CO_3^{2-} and H_2O by Raman spectroscopy. *Geochim. Cosmochim. Acta* **90**, 1–11.

Ghosh P., Adkins J., Affek H., Balta B., Guo W., Schauble E. A., Schrag D. and Eiler J. M. (2006) $^{13}C–^{18}O$ bonds in carbonate minerals: a new kind of paleothermometer. *Geochim. Cosmochim. Acta* **70**, 1439–1456.

Goetschl K. E., Purgstaller B., Dietzel M. and Mavromatis V. (2019) Effect of sulfate on magnesium incorporation in low-magnesium calcite. *Geochim. Cosmochim. Acta* **265**, 505–519.

Guo Y., Deng W. and Wei G. (2019) Kinetic effects during the experimental transition of aragonite to calcite in aqueous solution: Insights from clumped and oxygen isotope signatures. *Geochim. Cosmochim. Acta* **248**, 210–230.

Hendy C. H. (1971) The isotopic geochemistry of speleothems, I. The calculation of the effects of different modes of formation on the isotopic composition of speleothems and their applicability as paleoclimatic indicators. *Geochim. Cosmochim. Acta* **35**, 801–824.

Hill P. S., Tripati A. K. and Schauble E. A. (2014) Theoretical constraints on the effects of pH, salinity, and temperature on clumped isotope signatures of dissolved inorganic carbon species and precipitating carbonate minerals. *Geochim. Cosmochim. Acta* **125**, 610–652.

Hoefs J. (2015) *Stable Isotope Geochemistry*, seventh ed. Springer-Verlag, Berlin Heidelberg, p. 389.

Horita J. (2014) Oxygen and carbon isotope fractionation in the system dolomite-water-CO_2 to elevated temperatures. *Geochim. Cosmochim. Acta* **129**, 111–124.

Horita J., Ueda A., Mizukami K. and Takatori I. (1989) Automatic δD and $\delta^{18}O$ analyses of multi-water samples using H_2- and CO_2-water equilibration methods with a common equilibration set-up. *Appl. Radiat. Isot.* **40**, 801–805.

Immenhauser A., Schöne B. R., Hoffmann R. and Niedermayr A. (2016) Mollusc and brachiopod skeletal hard parts: Intricate archives of their marine environment. *Sedimentology* **63**, 1–59.

Jacob D. E., Wirth R., Agbaje O. B. A., Branson O. and Eggins S. M. (2017) Planktic foraminifera form their shells via metastable carbonate phases. *Nat. Commun.* **8**, 1265.

Jensen A. C. S., Imberti S., Parker S. F., Schneck E., Politi Y., Fratzl P., Bertinetti L. and Habraken W. J. E. M. (2018) Hydrogen bonding in amorphous calcium carbonate and molecular reorientation induced by dehydration. *J. Phys. Chem. C* **122**, 3591–3598.

Jin W., Jiang S., Pan H. and Tang R. (2018) Amorphous phase mediated crystallization: fundamentals of biomineralization. *Crystals* **8**, 48.

Katz A., Bonifacie M., Hermoso M., Cartigny P. and Calmels D. (2017) Laboratory-grown coccoliths exhibit no vital effect in clumped isotope (Δ_{47}) composition on a range of geologically relevant temperatures. *Geochim. Cosmochim. Acta* **208**, 335–353.

Kele S., Breitenbach S. F. M., Capezzuoli E., Meckler A. N., Ziegler M., Millan I. M., Kluge T., Deák J., Hanselmann K., John C. M., Yan H., Liu Z. and Bernasconi S. M. (2015) Temperature dependence of oxygen- and clumped isotope fractionation in carbonates: a study of travertines and tufas in the 6–95°C temperature range. *Geochim. Cosmochim. Acta* **168**, 172–192.

Kelson J. R., Huntington K. W., Schauer A. J., Saenger C. and Lechler A. R. (2017) Toward a universal carbonate clumped isotope calibration: diverse synthesis and preparatory methods suggest a single temperature relationship. *Geochim. Cosmochim. Acta* **197**, 104–131.

Kim S.-T. and O'Neil J. R. (1997) Equilibrium and nonequilibrium oxygen isotope effects in synthetic carbonates. *Geochim. Cosmochim. Acta* **61**, 3461–3474.

Kim S.-T., Hillaire-Marcel C. and Mucci A. (2006) Mechanisms of equilibrium and kinetic oxygen isotope effects in synthetic aragonite at 25°C. *Geochim. Cosmochim. Acta* **70**, 5790–5801.

Kimball J., Eagle R. and Dunbar R. (2016) Carbonate "clumped" isotope signatures in aragonitic scleractinian and calcitic gorgonian deep-sea corals. *Biogeosciences* **13**, 6487–6505.

Kluge T., John C. M., Boch R. and Kele S. (2018) Assessment of factors controlling clumped isotopes and $\delta^{18}O$ values of hydrothermal vent calcites. *Geochem. Geophys. Geosyst.* **19**, 1844–1858.

Kluge T., John C. M., Jourdan A.-L., Davis S. and Crawshaw J. (2015) Laboratory calibration of the calcium carbonate clumped isotope thermometer in the 25–250°C temperature range. *Geochim. Cosmochim. Acta* **157**, 213–227.

Konrad F., Gallien F., Gerard D. E. and Dietzel M. (2016) Transformation of amorphous calcium carbonate in air. *Cryst. Growth Des.* **16**, 6310–6317.

Konrad F., Purgstaller B., Gallien F., Mavromatis V., Gane P. and Dietzel M. (2018) Influence of aqueous Mg concentration on the transformation of amorphous calcium carbonate. *J. Cryst. Growth* **498**, 381–390.

Kosednar-Legenstein B., Dietzel M., Leis A. and Stingl K. (2008) Stable carbon and oxygen isotope investigation in historical lime mortar and plaster – results from field and experimental study. *Appl. Geochem.* **23**, 2425–2437.

Leukel S., Panthöfer M., Mondeshki M., Kieslich G., Wu Y., Krautwurst N. and Tremel W. (2018) Mechanochemical access to defect-stabilized amorphous calcium carbonate. *Chem. Mater.* **30**, 6040–6052.

Levitt N. P., Eiler J. M., Romanek C. S., Beard B. L., Xu H. and Johnson C. M. (2018) Near equilibrium $^{13}C–^{18}O$ bonding during inorganic calcite precipitation under chemo-stat conditions. *Geochem. Geophys. Geosyst.* **19**, 901–920.

Loste E., Wilson R. M., Seshadri R. and Meldrum F. C. (2003) The role of magnesium in stabilising amorphous calcium carbonate and controlling calcite morphologies. *J. Cryst. Growth* **254**, 206–218.

Mass T., Giuffre A. J., Sun C. Y., Stifler C. A., Frazier M. J., Neder M., Tamura N., Stan C. V., Marcus M. A. and Gilbert P. U. P. A. (2017) Amorphous calcium carbonate particles form coral skeletons. *PNAS* **114**, E7670–E7678.

Mavromatis V., Gautier Q., Bosc O. and Schott J. (2013) Kinetics of Mg partition and Mg stable isotope fractionation during its incorporation in calcite. *Geochim. Cosmochim. Acta* **114**, 188–203.

Mavromatis V., Purgstaller B., Dietzel M., Buhl D., Immenhauser A. and Schott J. (2017a) Impact of amorphous precursor phases on magnesium isotope signatures of Mg-calcite. *Earth Planet. Sci. Lett.* **464**, 227–236.

Mavromatis V., Immenhauser A., Buhl D., Purgstaller B., Baldermann A. and Dietzel M. (2017b) Effect of organic ligands on Mg partitioning and Mg isotope fractionation during low-temperature precipitation of calcite in the absence of growth rate effects. *Geochim. Cosmochim. Acta* **207**, 139–153.

Mavromatis V., Schmidt M., Botz R., Comas-Bru L. and Oelkers E. H. (2012) Experimental quantification of the effect of Mg on calcite-aqueous fluid oxygen isotope fractionation. *Chem. Geol.* **310–311**, 97–105.

McCrea J. M. (1950) On the isotopic chemistry of carbonates and a paleotemperature scale. *J. Chem. Phys.* **18**, 849–857.

Müller I. A., Rodriguez-Blanco J. D., Storck J.-C., do Nascimento G. S., Bontognali T. R. R., Vasconcelos C., Benning L. G. and Bernasconi S. M. (2019) Calibration of the oxygen and clumped isotope thermometers for (proto-)dolomite based on synthetic and natural carbonates. *Chem. Geol.* **525**, 1–17.

Nebel H., Neumann M., Mayer C. and Epple M. (2008) On the structure of amorphous calcium carbonate – a detailed study by solid-state NMR spectroscopy. *Inorg. Chem.*, 7874–7879.

O'Neil J. R., Clayton R. N. and Mayeda T. K. (1969) Oxygen isotope fractionation in divalent metal carbonates. *J. Chem. Phys.* **51**.

Owen R., Kennedy H. and Richardson C. (2002) Isotopic partitioning between scallop shell calcite and seawater: effect of shell growth rate. *Geochim. Cosmochim. Acta* **66**, 1727–1737.

Parkhurst D. L. and Appelo C. A. J. (1999) User's guide to PHREEQC (version 2); a computer program for speciation, batch-reaction, one-dimensional transport, and inverse geochemical calculations. *Water-Resour. Invest. U.S. Geol. Sur.*, 312.

Piasecki A., Bernasconi S. M., Grauel A. L., Hannisdal B., Ho S. L., Leutert T. J., Marchitto T. M., Meinicke N., Tisserand A. and Meckler N. (2019) Application of clumped isotope thermometry to benthic foraminifera. *Geochem. Geophys. Geosyst.* **20**, 2082–2090.

Prus M., Szymanek K., Mills J., Nielsen Lammers L., Piasecki W., Kedra-Królik K. and Zarzycki P. (2019) Electrophoretic and potentiometric signatures of multistage $CaCO_3$ nucleation. *J. Colloid Interface Sci.*.

Purgstaller B., Goetschl K. E., Mavromatis V. and Dietzel M. (2019) Solubility investigations in the amorphous calcium magnesium carbonate system. *CrystEngComm* **21**, 155–164.

Purgstaller B., Konrad F., Dietzel M., Immenhauser A. and Mavromatis V. (2017) Control of Mg^{2+}/Ca^{2+} activity ratio on the formation of crystalline carbonate minerals via an amorphous precursor. *Cryst. Growth Des.* **17**, 1069–1078.

Purgstaller B., Mavromatis V., Immenhauser A. and Dietzel M. (2016) Transformation of Mg-bearing amorphous calcium carbonate to Mg-calcite – In situ monitoring. *Geochim. Cosmochim. Acta* **174**, 180–195.

Révész K. M. and Landwehr J. M. (2002) $\delta^{13}C$ and $\delta^{18}O$ isotopic composition of $CaCO_3$ measured by continuous flow isotope ratio mass spectrometry: statistical evaluation and verification by application to Devils Hole core DH-11 calcite. *Rapid Commun. Mass Spectrom.* **16**, 2102–2114.

Rodriguez-Blanco J. D., Shaw S. and Benning L. G. (2015) A route for the direct crystallization of dolomite. *Am. Mineral.* **100**, 1172–1181.

Sade Z. and Halevy I. (2017) New constraints on kinetic isotope effects during $CO_{2(aq)}$ hydration and hydroxylation: revisiting theoretical and experimental data. *Geochim. Cosmochim. Acta* **214**, 246–265.

Schauble E. A., Ghosh P. and Eiler J. M. (2006) Preferential formation of ^{13}C–^{18}O bonds in carbonate minerals, estimated using first-principles lattice dynamics. *Geochim. Cosmochim. Acta* **70**, 2510–2529.

Schmidt M., Xeflide S., Botz R. and Mann S. (2005) Oxygen isotope fractionation during synthesis of Ca-Mg carbonate and implications for sedimentary dolomite formation. *Geochim. Cosmochim. Acta* **69**, 4665–4674.

Ševčík R., Mácová P., Sotiriadis K., Pérez-Estébanez M., Viani A. and Šašek P. (2016) Micro-Raman spectroscopy investigation of the carbonation reaction in a lime paste produced with a traditional technology. *J. Raman Spectrosc.* **47**, 1452–1457.

Spero H. J. and Lea D. W. (1996) Experimental determination of stable isotope variability in Globigerina bulloides: implications for paleoceanographic reconstructions. *Mar. Micropaleontol.* **28**, 231–246.

Spooner P.-T., Weifu G., Robinson L. F. and Leng M. J. (2016) Clumped isotope composition of cold-water corals: a role for vital effects? *Geochim. Cosmochim. Acta* **179**, 123–141.

Spötl C. and Vennemann T. W. (2003) Continuous-flow isotope ratio mass spectrometric analysis of carbonate minerals. *Rapid Commun. Mass Spectrom.* **17**, 1004–1006.

Stolper D. A. and Eiler J. M. (2015) The kinetics of solid-state isotope-exchange reactions for clumped isotopes: a study of inorganic calcites and apatites from natural and experimental samples. *Am. J. Sci.* **315**, 363–411.

Tang J., Dietzel M., Fernandez A., Tripati A. K. and Rosenheim B. E. (2014) Evaluation of kinetic effects on clumped isotope fractionation (Δ_{47}) during inorganic calcite precipitation. *Geochim. Cosmochim. Acta* **134**, 120–136.

Tarutani T., Clayton R. N. and Mayeda T. K. (1969) The effect of polymorphism and magnesium substitution on oxygen isotope fractionation between calcium carbonate and water. *Geochim. Cosmochim. Acta* **33**, 987–996.

Tripati A. K., Hill P. S., Eagle R. A., Mosenfelder J. L., Tang J., Schauble E. A., Eiler J. M., Zeebe R. E., Uchikawa J., Coplen T. B., Ries J. B. and Henry D. (2015) Beyond temperature: clumped isotope signatures in dissolved inorganic carbon species and the influence of solution chemistry on carbonate mineral composition. *Geochim. Cosmochim. Acta* **166**, 344–371.

Uchikawa J. and Zeebe R. E. (2013) No discernible effect of Mg^{2+} ions on the equilibrium oxygen isotope fractionation in the CO_2–H_2O system. *Chem. Geol.* **343**, 1–11.

Urey H. C. (1947) The thermodynamic properties of isotopic substances. Liversidge lecture, delivered before the Chemical Society in the Royal Institution on December 18th, 1946. *J. Chem. Soc. (Resumed)*, 562–581.

Usdowski E., Michaelis J., Böttcher M.-E. and Hoefs J. (1991) Factors of the oxygen isotope equilibrium fractionation between aqueous CO_2, carbonic acid, bicarbonate, carbonate and water (19°C). *Z. Phys. Chem.* **170**, 237–249.

Veizer J., Ala D., Azmy K., Bruckschen P., Buhl D., Bruhn F., Carden G. A. F., Diener A., Ebneth S., Godderis Y., Jasper T., Korte C., Pawellek F., Podlaha O. G. and Strauss H. (1999) $^{87}Sr/^{86}Sr$, $\delta^{13}C$ and $\delta^{18}O$ evolution of Phanerozoic seawater. *Chem. Geol.* **161**, 59–88.

Watkins J. M. and Hunt J. D. (2015) A process-based model for non-equilibrium clumped isotope effects in carbonates. *Earth Planet. Sci. Lett.* **432**, 152–165.

Watkins J. M., Hunt J. D., Ryerson F. J. and DePaolo D. J. (2014) The influence of temperature, pH, and growth rate on the $\delta^{18}O$ composition of inorganically precipitated calcite. *Earth Planet. Sci. Lett.* **404**, 332–343.

Watkins J. M., Nielsen L. C., Ryerson F. J. and DePaolo D. J. (2013) The influence of kinetics on the oxygen isotope composition of calcium carbonate. *Earth Planet. Sci. Lett.* **375**, 349–360.

Weise A. and Kluge T. (2019) Isotope exchange rates in dissolved inorganic carbon between 40°C and 90°C. *Geochim. Cosmochim. Acta* **268**, 56–72.

Zaarur S., Affek H. P. and Brandon M. T. (2013) A revised calibration of the clumped isotope thermometer. *Earth Planet. Sci. Lett.* **382**, 47–57.

Zeebe E. and Wolf-Gladrow D. (2005) *CO_2 in Seawater: Equilibrium, Kinetics*. Isotopes Elsevier, Amsterdam.

Associate editor: Claire Rollion-Bard